

DAMAGE TOLERANCE OF A CURVED COMPOSITE STIFFENED PANEL FABRICATED BY AN OUT OF AUTOCLAVE – LIQUID RESIN INFUSION PROCESS

D. Fanteria¹, L. Boni¹ & F. Romano²

¹University of Pisa - Department of Civil and Industrial Engineering – Aerospace Section
Via G. Caruso, 8 – 56126 Pisa – Italy; e-mail: daniele.fanteria@unipi.it

²CIRA S.C.p.A., Italian Aerospace Research Centre, Aeronautics - Technologies Integration Office.Via Maiorise, snc, 81043, Capua (CE), Italy.

Abstract

This paper presents the results of tests conducted on a curved stiffened panel to evaluate its damage tolerance capabilities. The panel was made from dry carbon preforms using Liquid Resin Infusion (LRI) followed by an Out-of-Autoclave curing. Non-linear Finite Element analysis results are also presented and compared to the measurements. The research was funded by Clean Sky 2 JU, under EU H2020 RIP, GA No 807089 (Work Area Leader: Leonardo Aircraft).

Keywords: AoA-Liquid Resin Infusion composites, composite stiffened panel testing, Damage Tolerance of composite structures, Finite Element analysis

1. Introduction

Traditional prepreg based composites are the natural choice for primary structural applications in civil aircraft. This is due to their superior specific strength and specific stiffness. However, this improved performance comes at a higher cost, mainly due to the autoclave curing process and handling and storage issues. The latter have been addressed in the last years by developing new technologies employing dry carbon preforms and two component resins mixed just before their use. Further costs can be saved by avoiding the use of an autoclave, e.g. by using heated moulds (as in resin transfer moulding) or an oven (foregoing the potential benefits of pressure in ensuring high quality composite parts).

As a core-partner of the Regional Aircraft IADP in the H2020 Clean Sky 2 program, AIRGREEN 2 Cluster developed innovative manufacturing processes for aircraft primary structures in carbon/epoxy composites. Additionally, relevant design methods were developed and experimental verification on typical components conducted by members of the Cluster. A curved panel reinforced by inverted 'T' stringers was chosen as one of the reference structures. This panel represents the upper skin of the outer wing box of a regional passenger aircraft, specifically a 90-seat high wing turboprop that is intended as an enlarged development of the ATR72. The panel was designed using the developed methods and specifically derived material allowables. Dry carbon fibre preforms were used for lamination, and Liquid Resin Infusion (LRI) was used for the curing process, which was done in an oven (Out-of-Autoclave or OoA). Recently, similar fabrication processes have gained significant attention due to their demonstrated improvement in material quality and mechanical properties [1, 2].

The paper presents the results of experimental activities on the curved panel conducted at the Aerospace Structures and Materials Laboratory of the University of Pisa. The University of Pisa participated in the Clean Sky 2 program as a partner of the AIRGREEN 2 Cluster. The paper also presents the results of Finite Element analyses, which are compared to the measurements acquired during the tests.

2. Damage Tolerance and fatigue of aeronautical composite structures

In the context of civil aircraft certification, damage tolerance requirements prescribe the complex of engineering evaluations of primary structures intended to ensure that, should fatigue, corrosion, manufacturing defects or accidental damage occur during the operational life of the aircraft, the remaining structure can sustain reasonable loads without failure (or excessive deformation) until the damage is detected and repaired.

For civil aircraft certification, damage is defined as critical if it reduces the residual strength of the component to its maximum operating load or Limit Load (LL). It is therefore necessary to detect damage (during routine inspections) before it becomes critical. The ability to detect a flaw is determined by its type, shape, location and inspection method, so there is a detectability threshold. A damaged structure with defects below this threshold must withstand the Ultimate Load (UL), which is obtained by multiplying the Limit Load by a prescribed safety factor (1.5 for civil aircraft).

Unlike their metallic counterparts, composite structures are virtually insensitive to fatigue and damage tends not to propagate under service loading. In terms of damage, composites are extremely sensitive to impacts which, even at moderate energies and speeds, can significantly reduce the compressive strength of laminated shells and thin-walled stiffened lightweight structures.

The damage tolerance of composite structures depends on a) the loss of compressive strength caused by the impact (proportional to the impact energy) and b) the detectability of the impact damage associated with a particular inspection method. With regard to the latter point, the regulations focus mainly on visual inspection and therefore impact detection is related to the permanent indentation on the structure and damage severity is related to the depth of such indentation. Specific levels of damage are defined in terms of indentation, namely:

- The barely visible impact damage (BVID), which is the smallest damage detectable by a detailed visual inspection and is usually associated with a 0.5 mm deep permanent indentation [].
- The visible impact damage (VID), which is the smallest damage detectable under standard inspection conditions (less accurate than a detailed visual inspection). A 2 mm indentation is generally used to define the VID (alternatively a 20 mm perforation is used).

Residual compressive strength can also be related to permanent indentation after impact and three DT design regions can be defined for a structure:

- 1. The undetectable damage area (below BVID), for which the structure must withstand UL.
- 2. The detectable damage area (between BVID and VID), for which the structure must withstand LL.
- 3. The obviously detectable damage area (above VID), for which the structure must withstand flight loads and, depending on the severity of the damage, function as normally as possible.

The BVID is often the most critical in the DT certification of a composite aircraft structure: a structure with a BVID must withstand the UL throughout the life of the aircraft. It must also be demonstrated that the BVID does not grow under normal operating conditions, i.e. after a number of load cycles representative of an entire service life.

To account for this condition in the design, compression after impact (CAI) tests are performed to determine the compression knockdown factors to be applied, in addition to factors to account for the statistical scatter of material properties and the adverse effects of hot wet ambient conditions. A nogrowth condition is assumed for BVID, which must be validated by fatigue testing. Ultimately, the fatigue test aims to demonstrate that a structure representative of minimum quality (with maximum tolerated manufacturing defects and damage) will retain its ultimate load capacity throughout its service life.

In defining the amplitude of the test fatigue cycles and their number scatter associated with fatigue behavior must be considered and appropriate simplifications introduced to facilitate the test. For components such as the panel of this research, constant amplitude cycles are normally considered with an amplitude such that a single cycle is representative (equally damaging in the language of fatigue) of a flight; amplitude factorization via a Load Enhancement Factor (LEF) can be introduced together with a Life Factor to manage the scatter while maintaining a reasonable duration of the tests (maximum number of cycles to be applied to be representative of real life use).

3. Design and fabrication of the test panel

3.1 Panel design

A curved panel (Tool side radius of curvature equal to 2981 mm) has been designed that is stiffened by inverted "T" stringers having their general dimension as reported in the sketch shown in Figure 1a. FE models were developed to support a no-buckling design of a 3 ribs (spacing 320 mm) 3 stringers/4spacing width panel.

The general arrangement of the layup for the stiffening members layup is shown Figure 1b while the stacking sequence is given in Table 1.

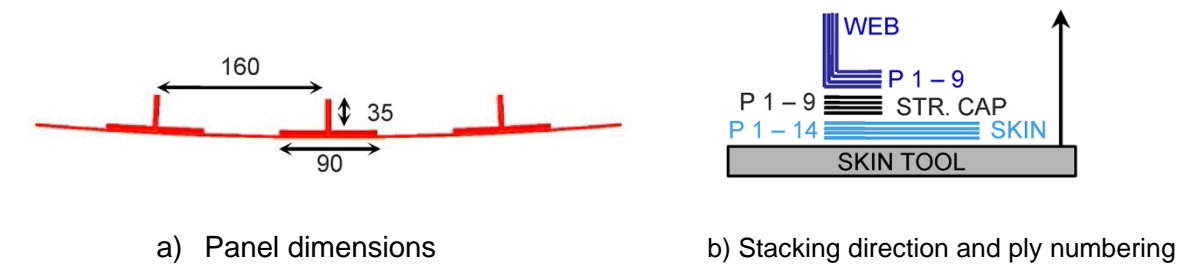


Figure 1 – Curved panel dimensions and stacking directions of the structural elements.

FE analyses were carried out to determine buckling loads and first ply failure load according to material data and design allowables determined using CAI knock-down factors. Analyses with a simply supported skin along the side straight edges and a grounded skin in correspondence to rib feet (i.e. ribs were not included in the model) showed a failure load of 540 kN and a buckling load of 760 kN,

Item	# of plies	Stacking sequence
Skin	14	45/-45/0/0/90/-45/45/45/-45/90/0/0/-45/45
Stringer Cap	9	45/-45/0/0/90/-45/45/-45/45
Stringer web	9	45/-45/45/-45/90/0/0/-45/45

Table 1 – Staking sequences.

3.2 Fabrication via LRI/OoA process

The panel is manufactured from dry carbon preforms by means of vacuum assisted Liquid Resin Infusion and an oven (Out-of-Autoclave) curing process [1-3].

The curing tool consists of a formed steel sheet offering a layup surface with a 2981mm curvature radius that is the OML of the curved panel. The tool surface is screwed to a steel framework supporting structure.

Appropriate mandrels for the forming of the stringers are connected to the skin tool via pins that allow relative sliding during the resin infusion and the curing process.

Dry non-crimp fabric is Hand lay up (HLU) and preformed (under vacuum and heat) prior to infusion. Then the internal and external vacuum bags are setup adding appropriate resin inlets and outlets for the resin infusion.

Prior to infusion the tool is preheated, and the resin (EP 24000) is preheated and degassed. Then infusion starts via inlets placed along the sides of the skin. Infusion proceeds until the resin reaches the outlet gates (placed along the webs of the stringers), then inlet gates are closed while the outlet gates remain connected to vacuum.

The panel is cured in an oven at ambient pressure and the curing cycle includes the following steps: a temperature increase (at 2°C/min) to 180°C, dwell for 120 min, cooling (at < 5°C/min) to 60°C or below. After debagging the panel is trimmed and drilled using a CNC milling equipment. Holes are drilled to allow the installation of dummy aluminum ribs that define the wing bays.

4. CS2 GRA Component testing: aims, protocols and requirements

The project included tests on intermediate components (elements/details) to validate the production methods and the numerical models for the analysis and structural design for the wing of a 90 pax regional aircraft. These intermediate tests were propaedeutic at the design, analysis, manufacturing and ground-testing of the full-scale composite Outer Wing Box (OWB) demonstrator programmed for a later stage of the project. The curved panel in question was part of this process together with tests performed also on a rib and a spar segment.

4.1 General aims and requirements for testing the AoA-LRI curved panel

The following general requirements are defined for the Curved Panel:

- The panel shall be compliant with the "no growth" approach for BVID damages, under compression-compression fatigue loading at constant amplitude.
- Implement suitable methods to identify the possible damage growth under fatigue loading
- A Design Service Goal (DSG) of 60000 flights, a 1.5 Life factor, and a 1.15 Load Enhancement Factor (LEF) shall determine the number of cycles and the maximum cyclic load.
- After the fatigue cycles the panel must retain a residual strength at least equal to the Design Ultimate Load (DUL).

4.2 Test protocol for mechanical testing (fatigue & static)

According to the general requirements and given the fact that a single tests article was available the following test protocol was applied. It consists of 6 steps:

- 1. Introduce BVID damages according to design and material response
- 2. Measure and mark damage extension prior to test via NDI
- 3. Install strain gauges in appropriate number and positions to effectively monitor possible changes in compliance due to damage growth
- 4. Apply the fatigue loading cycles in blocks and after each block perform a strain survey to check possible compliance variations
- 5. After all fatigue blocks have been applied perform a static compression test up to DUL while reading strain and end-shortening, then unload the panel
- 6. Perform a static compression test up to failure while reading strain and end-shortening

4.3 Specific requirements for the mechanical testing

In order to implement the selected test protocol, given the features of the test article and the general requirements, the following specific requirements had to be set for mechanical testing:

- 1. To have a uniform loading along panel width potted ends with precision milled faces are needed
- 2. Due to a 3 stringers/4 spacing width design side support fixtures are needed to avoid premature skin buckling of the straight edges
- 3. Design hypothesis for boundary conditions at ribs feet are hard to meet in practice; alternative supports for the dummy ribs are needed
- 4. Effective UL of the test article must be re-evaluated according to buckling loads resulting from test boundary conditions; LL shall be scaled accordingly to maintain consistency

5. Impact energy calibration, damage introduction and ultrasonic inspection

To evaluate the Damage Tolerance (DT) characteristics of the panel different impact damages were introduced. The panel was impacted using a pneumatic gun made available by Leonardo at Pomigliano D'arco company premises. An overview of damage locations and relevant parameters are given in Figure 2. Some trials were conducted (IDs with prefix A) to decide the energy level to produce Barely Visible Impact Damage at mid-bay (02 and 04) and under the stringer (01 and 03) locations. Since a spare panel was not available to calibrate the impact energies, trials were conducted on the lowermost bays as shown in figure 2.

Impact type	ID	Energy [J]	Depth [mm]
	A01	120	0.38
Calibration	A02	50	0.18
Calibration	A03	160	0.51
	A04	60	1.58
Official	B01	160	0.55
Official	B02	45	0.17

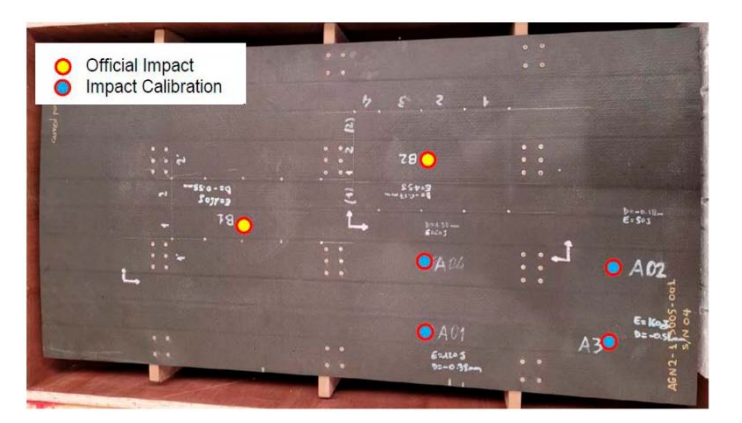


Figure 2 – Impact damage introduction.

After the execution of impacts, a state-of-the-art Ultrasonic Scanning (US) with a phased array probe was carried out to assess delaminated areas (Figure 3). An extended delamination, separating the stringer cap from the skin, was detected in correspondence of the BVID impact under the central stringer.

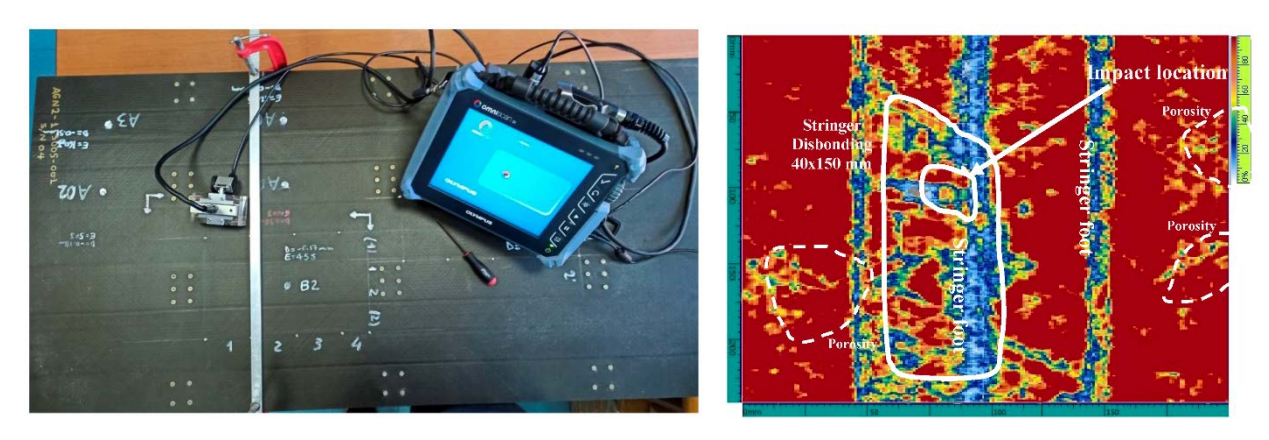


Figure 3 – NDI via phased array ultrasonic scanning.

6. Design of the test and associated test fixtures

Due to design constraints, specific fixtures were developed to provide side supports in addition to the supports for the ribs normally required in similar setups with wider test panels. Detailed Finite Element (FE) models and relative Non-linear analyses were developed (see figure 4) to define the test setup and to help design the fixtures.

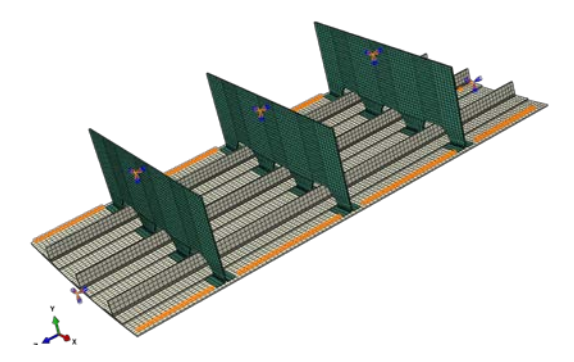
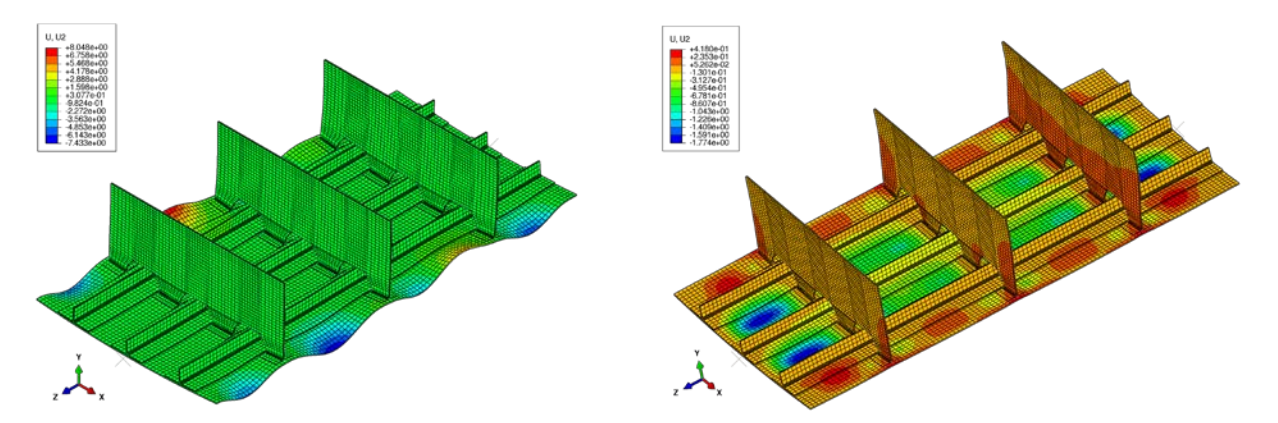


Figure 4 – FE model to guide the design of the test fixtures.

Due to a 3 stringers/4 spacing width design side support fixtures were needed to avoid premature skin buckling at the straight edges. Figure 5a show the first buckling mode in the case of free edges which occurs at an axial load approximatively equal to one third of the nominal design buckling load.

The buckling load was re-evaluated, considering the tests boundary conditions (i.e. with side supports and built-in edges of the dummy ribs) by means of virtual SG on an ABAQUS continuum shell model:

it was found at about 500 kN for pristine condition (no damage).



a) Buckling mode without side supports

b)Post-buckling deformation (side supports + built-in ribs)

Figure 5 – Non-linear FE results of the pristine panel with different boundary conditions.

The finite element (FE) models were also used to identify the best position for the strain gauges (SGs) to enhance the detection of possible delamination growth through strain surveys during testing.

6.1 Testing fixtures design

The design of the side supports was inspired to the constraint scheme of the FE analysis and features a local side support of the skin in each longitudinal bay in which the edges are subdivided by the ribs. The side support concept is shown in Figure 6.

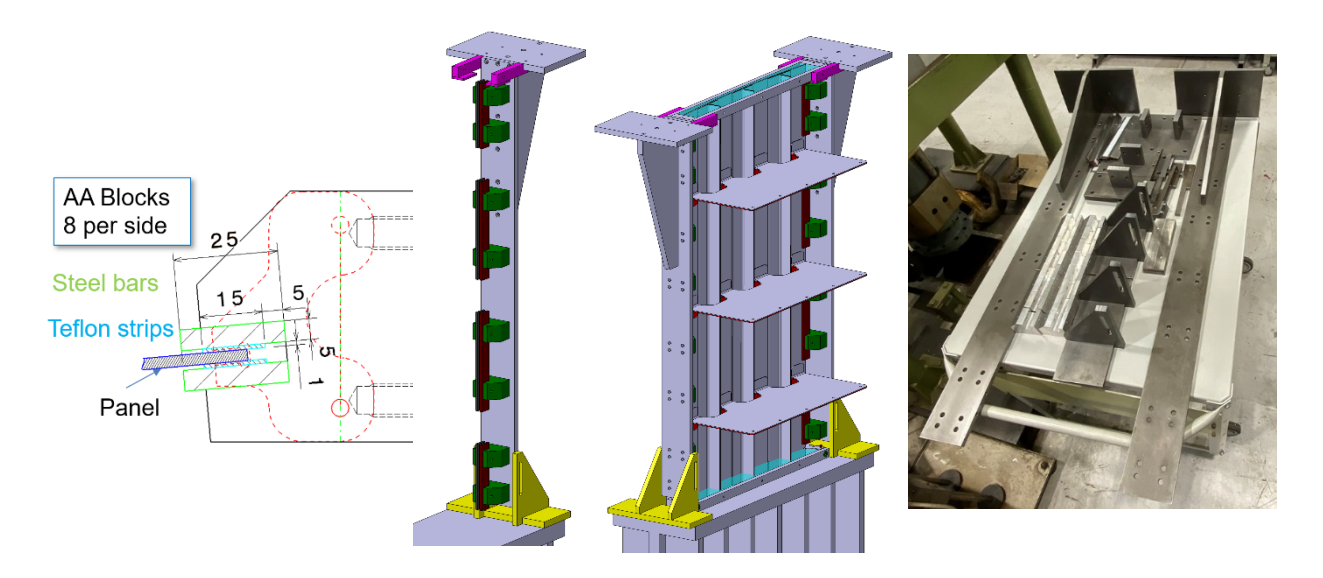


Figure 6. Side support concept, design and manufactured items ready to be installed

Each section of the edge of side skin is supported by steel bars that are held in place by a couple of AA alloy blocks fixed to side bars (one on each side of the panel). Teflon strips are interposed between the steel bars and the panel to ease local longitudinal sliding of the edge under axial deformation. Three-dimensional assembly drawings of the side supports are shown in Figure 6 together with the fixtures ready to be installed.

Supports for the dummy ribs were also designed to fix their edges to the frame of the testing machine through C section beams.

7. Preparation of the panel, test set-up and pre-load checks

Potted ends were casted using the frames supplied by the panel manufacturer. The panel was positioned with the stringers' axis orthogonal to a reference plane holding the end frame and equipped with columns restraining the panel during resin cast and cure. Potted ends were precision milled (see figure 7) to ensure planarity, reciprocal parallelism and orthogonality to the axes of the reinforcing stringers: this allows a uniform introduction of the load along the panel width.



Figure 7 – Installed potted ends after milling

Then 44 uniaxial strain gauges (SG) and 4 rosettes have been installed in back-to-back configuration. The test article mounted on a 3 MN Servo-Hydraulic fatigue testing machine is shown in figure 8.



Figure 8. Test set up completed and ready to start fatigue cycling.

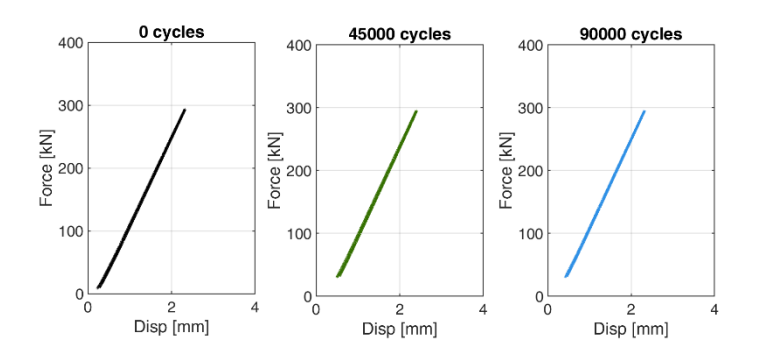
8. Fatigue testing results

Due to the re-evaluation of the buckling load (found equal to 500 kN), the Effective UL of the test article was set at 440 kN (13.6% margin) with the Effective LL equal to 293.3 kN (EUL/1.5).

Following Leonardo indication about the max cyclic load for a single equivalent cycle per flight (producing the same damage as all cycles in an average flight, representative of AC life), the maximum fatigue cyclic load has been assumed equal to LL (including a 1.15 LEF), with R=0.2. The total number of flights (and thus of Constant Amplitude cycles) is 90k (DSGx1.5).

Prior to starting fatigue cycling, preliminary loading was performed to check the uniformity of load introduction by checking the readings of SGs in the top half bay; minimal shimming was required to obtaining uniform loading.

The fatigue test was carried out at 0.5 Hz and stopped at 5k, 12k, 20k, 30k, 45k, 60k and 90k cycles for reading SGs and check possible compliance variations (indicative of damage growth). Axial load vs. end-shortening behaviour at 0, 45k and 80k cycles is reported in Figure 9 together with the panel axial stiffness (K) variation with fatigue cycles.



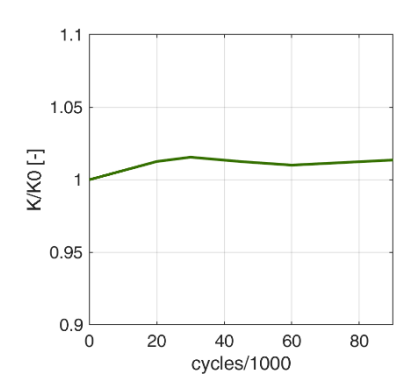


Figure 9. Variation of axial stiffness (K) with fatigue cycles Strain gauges installed in the vicinity of the stringer de-bond due to impact B1 show some secondary

bending at increasing axial load; this is expected at the edge of the de-bond and the specific readings have been monitored to check possible evolution with fatigue cycling. Strain reading in the vicinity of stringer de-bonding at LL for all strain surveys are shown in Figure 10 as a function of completed fatigue cycles.

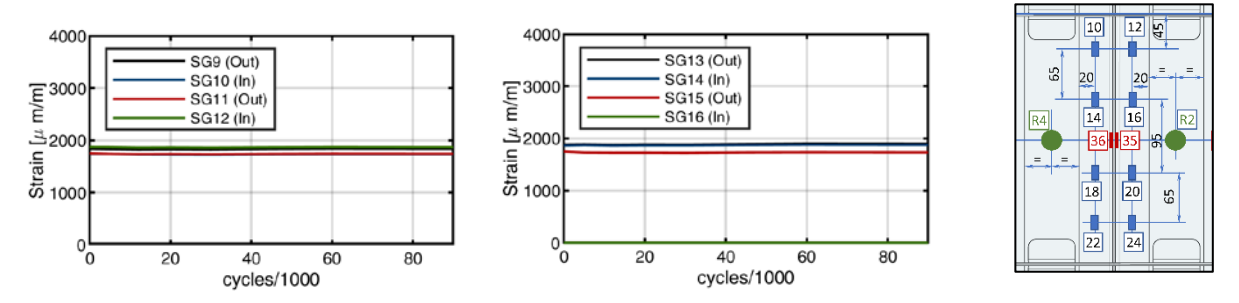


Figure 10. Variation of the SG reading in the vicinity of stringer de-bonding

The results confirm that any internal damage size did not change with fatigue cycling, or if it did, it did not cause significant stiffness variation, either globally or locally.

9. Damage tolerance capability and final static failure

After completing the 90k fatigue cycles the ultimate loading capability of the curved panel was demonstrated by applying a loading ramp at about 100 KN/min up to the DUL. As shown in the results presented in Figure 11 no failure occurred and the response of the panel in terms of strains was as expected. Some nonlinearities occurred for SG mounted close to the de-bond but strain levels remained below 4000 microstrains and all strains came back to zero upon load removal.

Then a static loading ramp (at the same lading rate of 100KN/min) was applied up to failure. Axial load vs. end-shortening behaviour is reported in Figure 11. The panel failed at an axial load of 457.6 KN that is about 4% more than its DUL

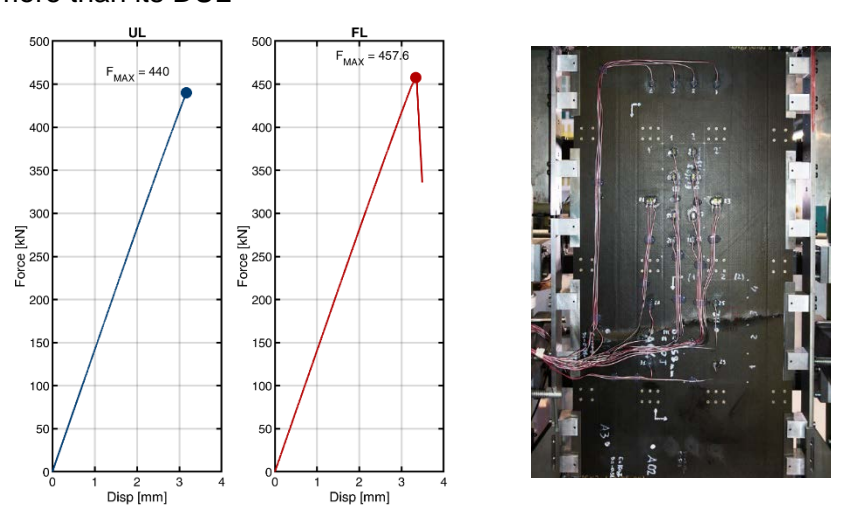


Figure 11. Axial load vs. end-shortening up to UL, and Failure Load (FL).

According to post-test images (an example is shown in figure 11) and strain gauge reading it is likely that failure was triggered by the interaction of skin buckling (appreciable in other inter-stringers bays) and the presence of damages due to trial impacts in the bottommost bay.

10. Non-linear Finite element analysis of compression tests

A more sophisticated FE model has been developed, which incorporates the initial de-bonding of the central stringer. Its outcomes have been compared to the strain data recorded during tests, which involved static loading for strain surveys between blocks of fatigue cycles or for verifying stiffness and strength capabilities.

In the numerical simulation the initial de-bonding at mid bay has been introduced in a region below the central stringer, extended about 150 mm in longitudinal direction (and extending for the whole width of the flange). Such a region is of rectangular shape, symmetrically distributed with respect to the stringer axis and only slightly shifted upwards from the bay centre-line. The effects of the geometrical non-linearity, which increase progressively up to the deep post-buckling regime, in this case interact with

the non-linearity introduced by the surface contact at de-bonded interface. The analysis, by accounting for the mutual influence among global post-buckling deformation and local skin-stringer separation due to de-bonding, allows to simulate more realistically the structural response of the compressed panel. The initial de-bonding has been modelled by locally replacing the skin-stringer tie constraint with a frictionless contact interaction between the faces, by allowing their separation. A finite-sliding contact with hard-separation algorithm has been used to simulate the complex alternation of surface interference and clearance which determine the final local deformation and, consequently, affects the global post-critical behaviour. The FE model is shown in figure 11 (left), where is evident the finer mesh in the panel portion affected by de-bonding. The out-of plane displacement induced by the initial defect is shown in the same figure (right).

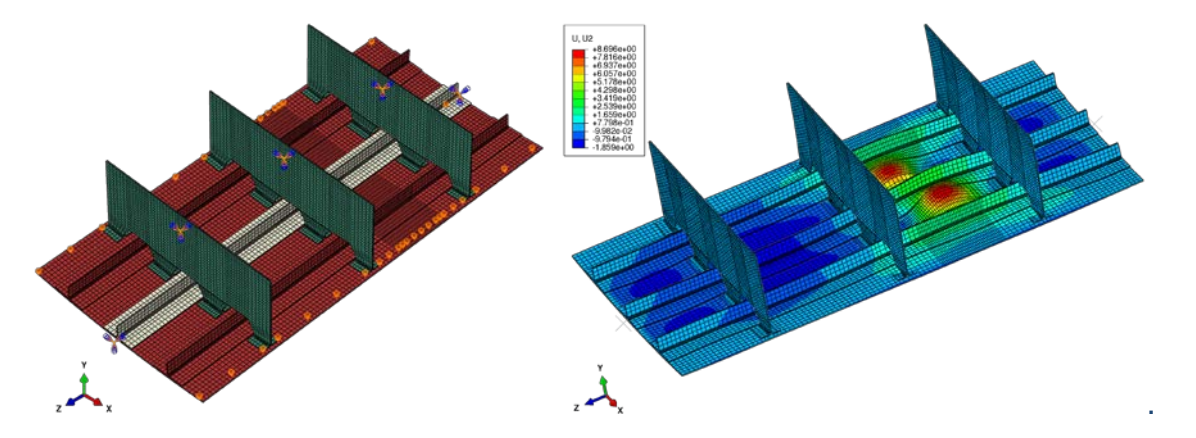


Figure 11. FE model with de-bonded stringer and out-of-plane displacement under load

The results provided by FEA are shown in terms of longitudinal strain vs applied load, extracted at the same locations of back-to-back strain gauges, mounted in surroundings of debonding region during tests (see the SG installation scheme reported in figures 12 and 13).

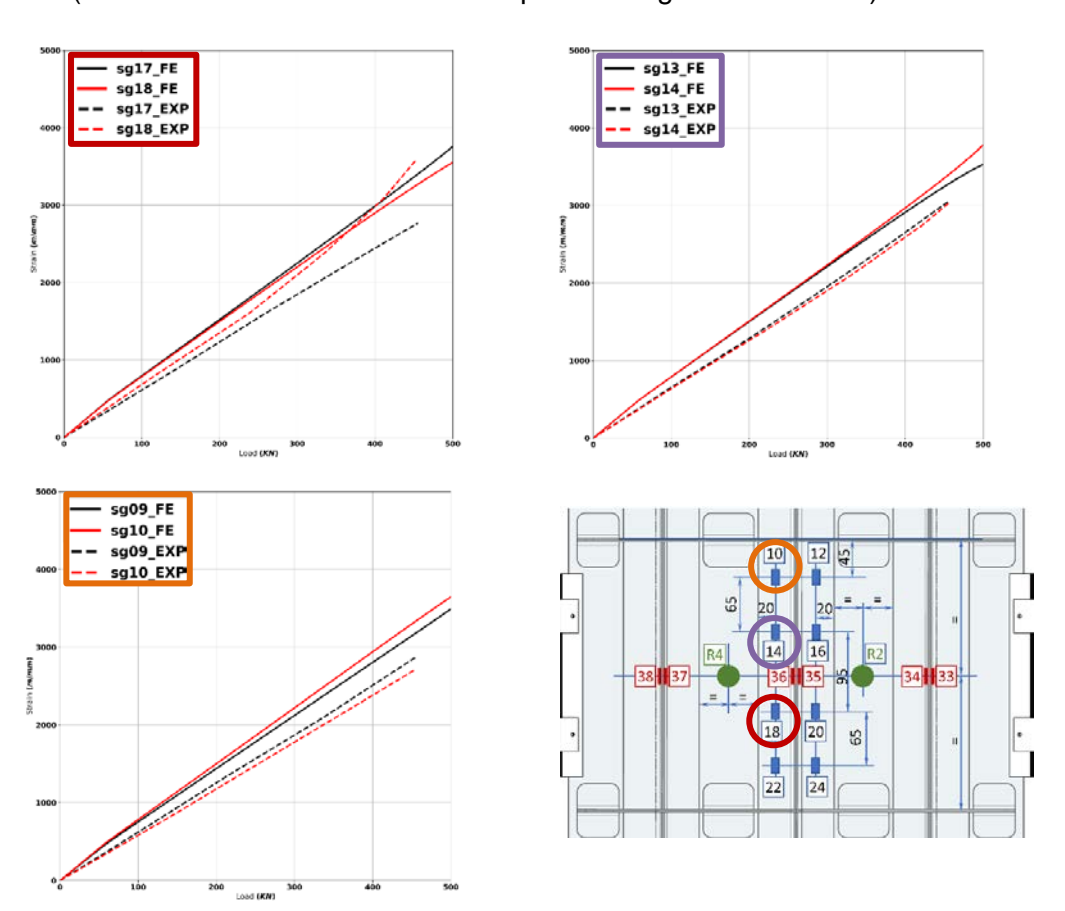


Figure 12. Comparison of numerically predicted vs. experimentally detected strains in the vicinity of the skin/stringer de-bond (skin side and stringer flange side).

In particular, the divergence from the mean compression between the strain on lower and upper surface indicates the occurrence of buckled regions. The numerical results are compared with those experimentally determined for different SG locations of skin or central stringer flange in figures 12 and stringer webs in figure 13.

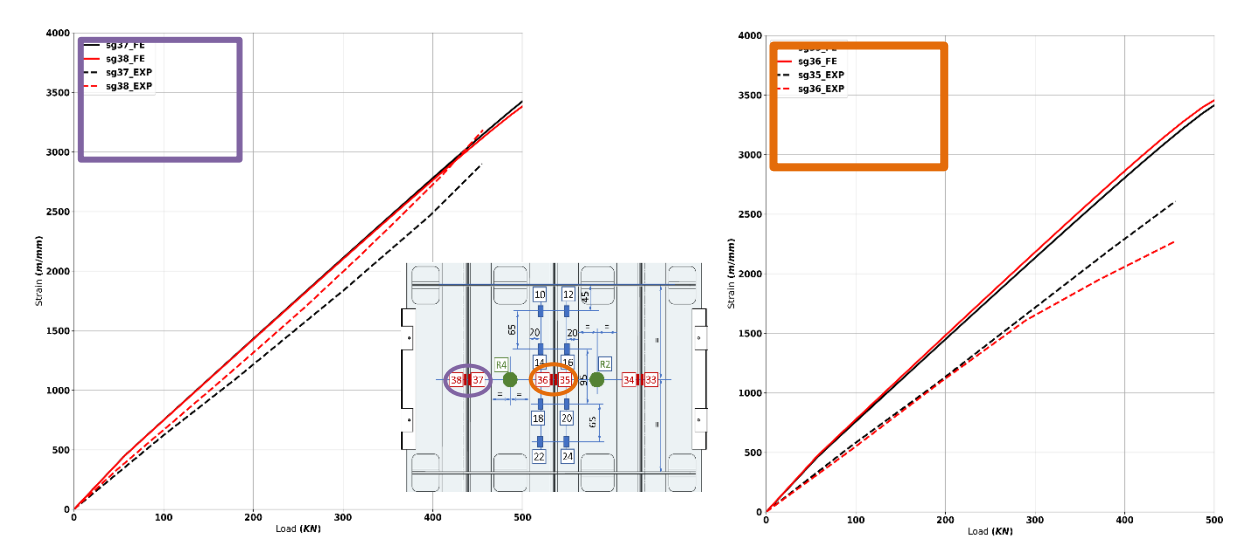


Figure 13. Comparison of numerically predicted vs. experimentally detected strains on stringers web locations.

The numerical and experimental data exhibit a good agreement, especially for the skin/stringer flange locations, where both global stiffness and buckling phenomena are quite well captured. The numerical simulation tends to overestimate the stiffness and to delay the buckling occurrence in the web of the central stringer, probably due to a slightly different stress redistribution in central part of de-bonding.

11. Conclusions

A curved panel, reinforced by inverted "T" stringers, fabricated by LRI/OoA process, has been analysed and tested. Prior to tests BVIDs were introduced and the internal damage assessed by means of US scanning.

The panel was able to sustain 90k fatigue cycles (about 1.5 the design service goal) without appreciable variation of either the global or local stiffnesses, thereby demonstrating the "no growth" approach for Damage Tolerance. After the fatigue cycles the panel was able to withstand Ultimate Load without failure and, in the subsequent loading, it reached 104% of UL before failure. The failure was triggered by the interaction of skin buckling with the presence of impact damage in the lower bay.

Non-Linear analyses including stringer de-bonding gave results in good agreement with experiments provided the post-buckling of the damaged zone is captured. This is because the results are sensitive to the initial shape, which may be influenced by the impact damage.

The results of the test would serve as a reference for tuning and validation of numerical predictions with models of increasing complexity: the ultimate goal is to validate models capable to simulate impact damage and predict damage evolution under fatigue loads.

12. Copyright Statement

The authors confirm that they, and/or their company or organization, hold copyright on all of the original material included in this paper. The authors also confirm that they have obtained permission, from the copyright holder of any third party material included in this paper, to publish it as part of their paper. The authors confirm that they give permission, or have obtained permission from the copyright holder of this paper, for the publication and distribution of this paper as part of the ICAS proceedings or as individual off-prints from the proceedings.

13. References

- [1] Karachalios, E., Muñoz, K., Jimenez, M., Prentzias, V., Goossens, S., Geernaert, T. and Plagi-anakos, T.S. LRI-fabricated composite demonstrators for an aircraft fuselage on the basis of a Building Block design approach. *Composites Part C: Open Access* 6 (2021) 100178.
- [2] Oosterom, S. van, Allen, T., Battley, M. and Bickerton, S. An objective comparison of common vacuum assisted resin infusion processes. *Composites Part A: Applied Science and Manufacturing* 125 (2019) 105528.
- [3] Singer, J., Arbocz, J., Weller, T. Buckling Experiments: Experimental Methods in Buckling of Thin-Walled Structures. Vol. 2: Shells, Built-up Structures, Composites and Additional Topics, Wiley, 2002.
- [4] Boni, L., Fanteria, D., Lanciotti, A. Post-buckling behaviour of flat stiffened composite panels: Experiments vs. analysis, Composite Structures (2012), 94 (12), pp. 3421-3433.